journal of the mechanical behavior of biomedical materials 146 (2023) 106077

Contents lists available at ScienceDirect

Journal of the Mechanical Behavior of Biomedical Materials

journal homepage: www.elsevier.com/locate/jmbbm

# Application of stacked autoencoder for identification of bone fracture

Dong-Yoon Kim [a], EunBin Park [a], KyoBeom Ku [a], Se Jin Hwang [b], Kyu Tae Hwang [c], Chang-Hun Lee [c], Gil Ho Yoon [a,*]

[a] School of Mechanical Engineering, Hanyang University, Seoul, South Korea
[b] Department of Anatomy and Cell Biology, College of Medicine, Hanyang University, Seoul, South Korea
[c] Department of Orthopaedic Surgery, College of Medicine, Hanyang University, Seoul, South Korea

ARTICLE INFO

*Keywords:*
Bone fracture
Transverse vibration
Frequency response function
Bilateral symmetry
Stacked autoencoder

ABSTRACT

This study presents a stacked autoencoder (SAE)-based assessment method which is one of the unsupervised learning schemes for the investigation of bone fracture. Relatively accurate health monitoring of bone fracture requires considering physical interactions among tissue, muscle, wave propagation and boundary conditions inside the human body. Furthermore, the investigation of fracture, crack and healing process without state-of-the-art medical devices such as CT, X-ray and MRI systems is challenging. To address these issues, this study presents the SAE method that incorporates bilateral symmetry of the human legs and low-frequency transverse vibration. To verify the presented method, several examples are employed with plastic pipes, cadaver legs and human legs. Virtual spectrograms, created by applying a short-time Fourier transform to the differences in vibration responses, are employed for image-based training in SAE. The virtual spectrograms are then classified and the fine-tuning is also carried out to increase the accuracy. Moreover, a confusion matrix is employed to evaluate classification accuracy and training validity.

## 1. Introduction

This research proposes a stacked autoencoder (SAE)-based assessment method using bilateral symmetry and transverse vibration responses to investigate a bone fracture of human legs. The human legs are not easy to diagnose without state-of-the-art medical devices, especially since it contains tissues, muscles and various boundary conditions. Moreover, it is more difficult to diagnose a fracture in an emergency or undeveloped environment. Considering these issues, in the presented study, SAE diagnosis method is developed with the concept of bilateral symmetry of the human legs and low-cost vibration testing equipment.

With the help of the development of medical science and technology, several imaging methods such as X-ray, computed tomography (CT) and magnetic resonance imaging (MRI) can be mainly used for orthopedic diagnosis (Nicholson et al., 2021; Thürig et al., 2022; Umans and Kaye, 1996; Chitkara et al., 2013). However, due to their high cost and radiation exposure, it is still difficult and potentially harmful for the daily monitoring of patient conditions (Sorriento et al., 2021; Mahesh, 2001; Ribeiro et al., 2020). The lack of biomechanical information in imaging methods can also lead to subjective diagnosis depending on the clinician's experiences (Bizzoca et al., 2020; Dos Santos et al., 2023; Cao et al., 2023; Barra and Boire, 2001). To complement existing imaging methods, alternative methods with analysis of mechanical vibration and electrical impedance have been studied (Conceição et al., 2022; Chiu et al., 2017; Alizad et al., 2006; Yoshida et al., 2009).

Since the recovery of fractured bone is a process of restoring its biological and mechanical properties, assessment of mechanical and dynamic characteristics of bone including its stiffness and strength increasing during this process can be a quantitative indicator for bone healing monitoring. To investigate the mechanical and dynamic characteristics, a vibration-based method is regarded as a promising technique as it is non-invasive and easy to collect vibration data reflecting the status of fractured bone (Bediz et al., 2010; Akkus et al., 1998; Mattei et al., 2021). In an undeveloped environment and emergency without medical devices, these vibration-based methods can be effectively utilized to diagnose bone fracture using the bilateral symmetrical characteristics of human and animal (Sim et al., 2021; Yoon et al., 2021; Shen et al., 2021; Caron et al., 2023). In addition, vibration-based abnormality detection techniques using deep learning or machine learning have been employed (Kim et al., 2022; Pan et al., 2023; Hosseinpour-Zarnaq et al., 2022). The machine learning-based random forest (RF) was also researched to investigate the various fault cases (Noshad et al., 2019). For the detection of bone fracture, the artificial neural network

* Correspondence to: Department of Mechanical Engineering, College of Engineering, Hanyang University, Seoul, South Korea.
*E-mail address:* ghy@hanyang.ac.kr (G.H. Yoon).

https://doi.org/10.1016/j.jmbbm.2023.106077
Received 16 June 2023; Received in revised form 2 August 2023; Accepted 13 August 2023
Available online 16 August 2023

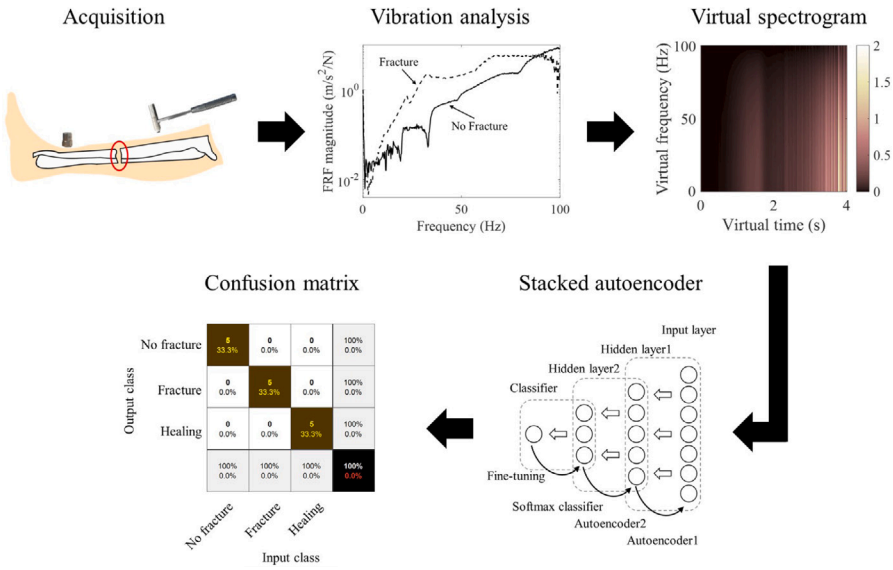


**Fig. 1.** Procedure of bone fracture diagnosis system using stacked autoencoder.

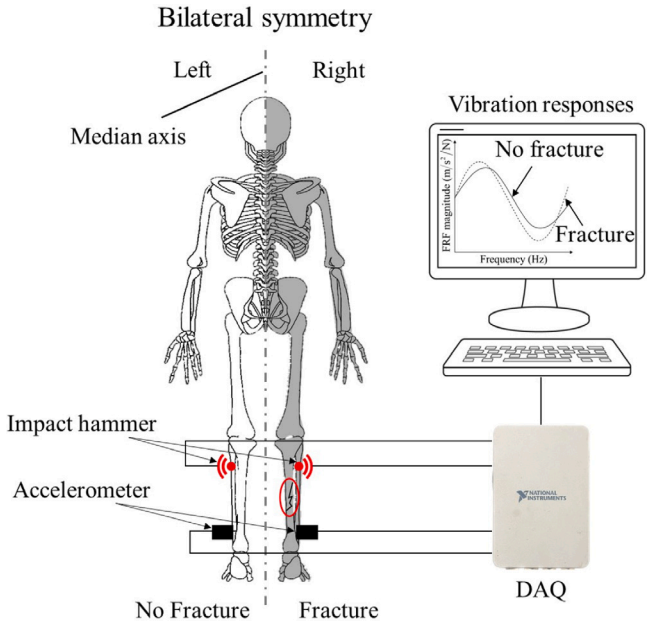


**Fig. 2.** Schematic of vibration experiment with bilateral symmetry of human body (With some differences, similar behaviors can be observed owing to the bilateral symmetry).

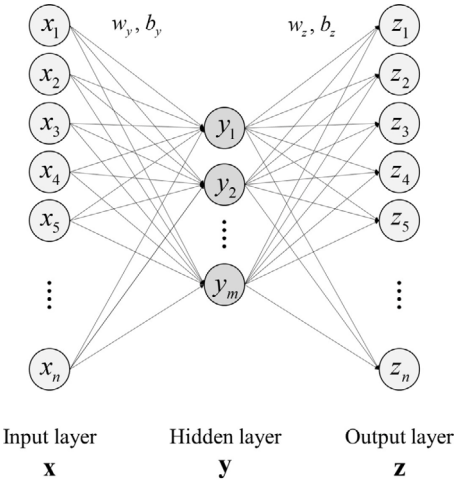


**Fig. 3.** Basic autoencoder scheme.

(ANN) method with line features of X-ray images was employed (Yang et al., 2019). Moreover, fractures of various bones in the human body are detected using a support vector machine and error backpropagation neural network (Bagaria et al., 2021). Imitation learning was researched to detect the vertebral compression fracture (Iyer et al., 2023). Among these methods, there are cases diagnosed with the autoencoder method which is unsupervised learning or the stacked autoencoder method which is unsupervised learning or semi-supervised learning (Zabalza et al., 2016; Adem et al., 2019; Lu et al., 2017; Yang et al., 2022).

Thus, the presented study employs the SAE to investigate the bone fracture of human legs with the concept of bilateral symmetry of human and transverse vibration responses of impact testing in Fig. 1. To carry out this method, plastic pipes, cadaver legs and human legs are employed. Moreover, the concept of virtual spectrograms transformed by the difference between frequency response functions is also used. In the SAE-based diagnosis system, the virtual spectrograms are classified with a confusion matrix.

The remainder of this paper is organized as follows. Section 2 provides the concept of the low-frequency vibration analysis for structural health monitoring and bilateral symmetry. The SAE incorporating the concept of virtual spectrograms is explained. Section 3 presents several examples including patient data are presented. Section 4 presents the conclusions of this study and provides suggestions for future research.

## 2. Low-frequency vibration analysis of structural health conditions

### 2.1. Vibration experiment with bilateral symmetry

From a medical and engineering point of view, it is intricate and difficult to obtain some reference vibration signals for damaged and undamaged bone in vivo. The dynamic characteristics of human are subject to be changed continuously by differentiating position, muscle force or body moisture. Therefore, utilizing the vibration data of patient for diagnosis purposes is very difficult. To address this issue, this

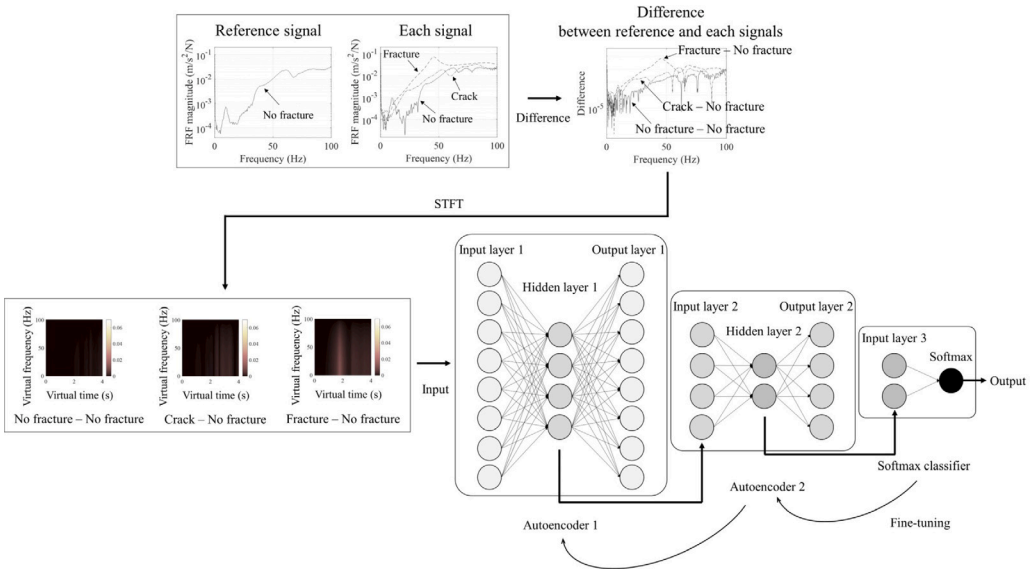


**Fig. 4.** Process of stacked autoencoder with virtual spectrograms.

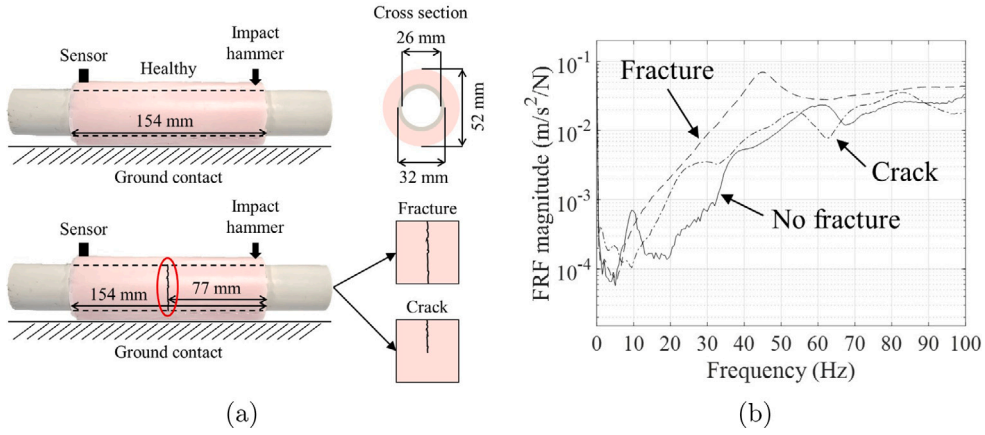


**Fig. 5.** Experiments of plastic pipe specimens covered with silicon. (a) The geometric configuration of plastic pipe specimens and (b) the FRFs without fracture, with fracture and crack.

subsection describes the utilization and exploration of the bilateral symmetry of human to investigate the structural health condition in Fig. 2. The bilateral symmetry of the human body is defined as the existence of symmetric anatomical parts arranged on opposite sides of the median axis. Some relevant research utilizing the bilateral symmetry exists (Sim et al., 2021; Yoon et al., 2021; Jacob and Wyawahare, 2013). The bilateral symmetry can provide references of healthy conditions and be utilized by medical professionals to improve the accuracy of diagnosis. Especially, it can be applied for the diagnosis of bone fracture, the healing process and pathological conditions. In this study, the bilateral symmetry is utilized as healthy condition can be diagnosed with non-invasive equipment environments by comparing the differences between the properties of health condition and those changed by fracture and degeneration.

Utilizing bilateral symmetry, transverse vibration experiments are conducted with plastic pipes, cadaver legs and human legs. For the vibration experiment, vibration responses are measured using an accelerometer (PCB 352C33), an impact hammer (PCB 086C03) and NI-9234 DAQ equipment in Fig. 2. In addition, the impact force ranges between 8 N and 14 N lower than the magnitude of force experienced in daily life. The sensitivity values of the impact hammer and the accelerometer are 12.02 mV/N and 1.044 mV/N/s$^2$, respectively. In the patient experiment, the force magnitude is enough to make vibrations safe to the patients. These measured vibration responses are converted into a frequency response function (FRF) and analyzed in the low-frequency domain. This FRF analysis is effective in confirming the eigenfrequency of each mode of the structure and the effect of damping. Note that different materials or structures have different vibration characteristics and therefore must be analyzed within the same system. In order to clarify the difference of vibration responses, the virtual spectrograms generated by the difference of FRFs are explained in the next subsection.

### *2.2. Stacked AutoEncoder(SAE) with virtual spectrograms — one of the AI-based diagnosis system (an unsupervised learning scheme)*

To rigorously diagnose the status of human bone, this subsection presents the application of a stacked autoencoder(SAE)-based diagnosis system with virtual spectrograms that are the 2-dimensional images data by applying the STFT for the difference between the frequency response functions (FRFs). Commonly, the supervised learning algorithm, i.e., CNN, has been researched for the detection of abnormality.

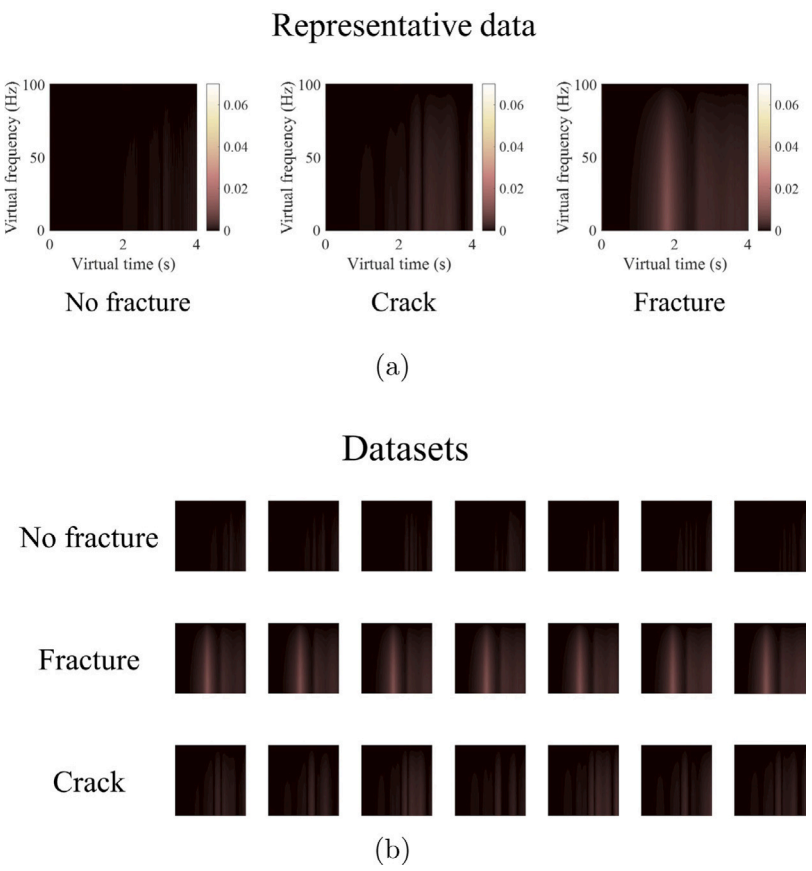


**Fig. 6.** Virtual spectrograms of the stacked autoencoder-based diagnosis system to identify the conditions of plastic pipes. (a) The representative virtual spectrograms of the three conditions without fracture, with fracture and crack and (b) the datasets of virtual spectrogram images used in the presented diagnosis system.

The supervised learning can achieve diagnosis more accurately than unsupervised learning. In some peculiar environments without state-of-the-art medical devices, the labeling process essential for supervised learning may not be possible. Therefore, in that case, unsupervised learning can be applied. In the present study, the unsupervised learning algorithm, i.e., the stacked autoencoder in this research, is applied. As mentioned, as the vibration signals are dependent on the condition of human, the bilateral symmetry is applied for a reference signal. The signals in the low-frequency range, i.e. around 100 Hz, contain valuable information regarding the status of bone (Sim et al., 2021; Yoon et al., 2021; He et al., 2017; Zhang et al., 2012). Although the investigation of the signals by medical doctor is a secured standard, recently, the classification relying on AI has been researched and becomes prominent. In the present study, the Stacked AutoEncoder (SAE), an AI-based diagnosis technique is applied to diagnose the condition of bone with the vibration data (Hinton and Salakhutdinov, 2006; Tao et al., 2015; Vařeka and Mautner, 2017; Khamparia et al., 2020).

A conventional autoencoder (AE) is a deep learning architecture model in which an original signal is inputted and reconstructed at the output, passing through an intermediate layer with a reduced number of hidden neurons (Kramer, 1991, 1992; Møller, 1993; Olshausen and Field, 1997). The AE model attempts to learn the abstract features in the reduced hidden neurons, enabling a reconstruction of the input signal from these features. A basic scheme of the AE is presented in Fig. 3. The input signals can be reduced to features in the hidden layer and reconstructed in the output layer. The training of an AE involves reproducing the input signals at the model's output. The internal units can then provide the original information. The values in the intermediate layer can be utilized as new reduced features to perform the reconstruction, representing the original signal. The AE is typically computed as follows:

$$\mathbf{y} = f(w_y\mathbf{x} + b_y) \tag{1}$$

$$\mathbf{z} = f(w_z\mathbf{y} + b_z) \tag{2}$$

$$\underset{w_y, w_z, b_y, b_z}{\arg\min}\ [error(\mathbf{x}, \mathbf{z})] \tag{3}$$

Where the value of the hidden layer $\mathbf{y}$ is obtained from the value of the input layer $\mathbf{x}$ by the weights $w_y$ and the bias $b_y$ in Eq. (1). The reconstructed value $\mathbf{z}$ from the input value is obtained from the output value $\mathbf{y}$ by the $w_z$ and the $b_z$ in Eq. (2). The function $f$ represents the activation function, which introduces non-linearity into the system. Eq. (3) is employed to determine the optimized parameters by minimizing the error between the $\mathbf{x}$ and the $\mathbf{z}$.

This concept can be expanded with the several layers between the input and the output layers in SAE. As complex networks and their classification require a network structure with more hidden layers, the SAE model can be obtained by connecting multiple autoencoders in succession. In this study, to diagnose the conditions of human legs, two autoencoders are used, followed by a softmax layer. The SAE is created by stacking and connecting two autoencoders with a hidden layer. With trial and error, it is found that the two layers are sufficient to classify the signals and the validations of hyperparameters are carried out beforehand in the subsequent examples. Some details of the employed SAE are as follows: The SAE uses 12–42 virtual spectrogram images (256 by 256 pixels) that represent the short-time Fourier transformation of the difference between reference data (vibration signals of healthy bone) and investigating data (vibration signals of healthy or fractured bone) for the training and test datasets, as shown in Fig. 4. The network consists of two autoencoder layers: Autoencoder 1 has a 128-node hidden layer, L2 weight regularization of 0.001, and sparsity proportion of 0.15, while Autoencoder 2 has a 64-node hidden layer, L2 weight regularization of 0.1, and sparsity proportion of 0.15. The network also includes a softmax layer and backpropagation is used to optimize the accuracy. The sparsity regularization is set to 4, and

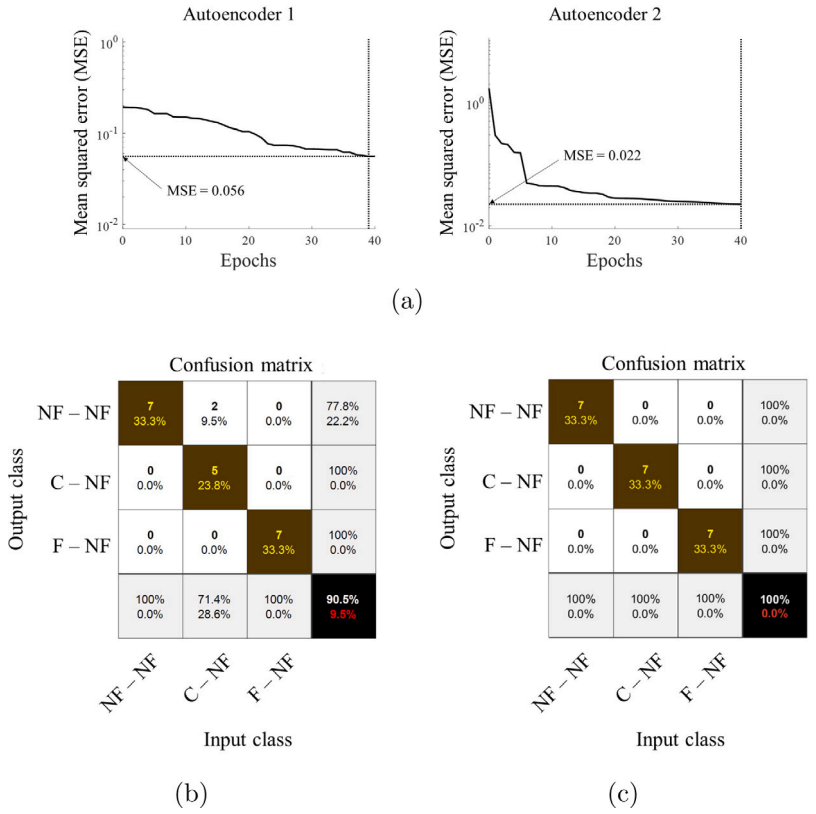


**Fig. 7.** Results of each process using the stacked autoencoder. (a) The mean squared errors(MSEs) of autoencoder 1 and autoencoder 2 with 40 epochs, (b) the confusion matrices of stacked autoencoder results testing the virtual spectrograms without the fine-tuning and (c) the confusion matrices of stacked autoencoder results testing the virtual spectrograms with the fine-tuning (NF: No fracture, F: Fracture and C: Crack).

40 epochs are used for training. The loss function in the softmax layer is cross-entropy. All algorithms are implemented in MATLAB R2021a (MATLAB, 2021).

## 3. Experimental results

To show the validity of the present stacked autoencoder(SAE)-based diagnosis method for human bone fracture detection, the four examples are considered. Typically, the detection of abnormalities has been predominantly explored using supervised learning algorithms. However, in this study, we have employed an unsupervised learning algorithm known as the SAE. As stated in the previous section, the virtual spectrograms are computed with the frequency response functions (FRFs) of healthy, fracture, crack and healing bones and models. By computing the confusion matrix showing the classification performance, the accuracy of the SAE algorithm is verified. First of all, the experiment with a plastic bar and silicon is considered for the verification. The two in-vivo tests (Cadaver's legs and real patient's legs) are also carried out.

### 3.1. Example 1: Plastic pipe specimens

Before applying the present SAE-based diagnosis system to the patient's bone, its application is investigated and verified with some artificial specimens. The three plastic pipes covered with silicon whose dimensions are presented in Fig. 5 are prepared. One of the plastic bars is healthy, while the other two specimens are fractured and cracked. One of the difficulties in the experiment is the uncertainty of the boundary condition as shown in Fig. 5(a). In other words, while it is easy to set boundary conditions in these simple pipe structures, i.e. simple straight structures, however, in the case of complex structures, especially for human legs, it is practically difficult to set the boundary condition accurately. In this study, the boundary condition of ground contact is adopted and the representative vibration curves of the three specimens are shown in Fig. 5(b). Fig. 5(b) shows the case-by-case averaged curves of multiple FRF curves. Less than 10 data for each case are used by excluding noisy data. It is observed that the magnitudes of the healthy specimen are lower than those of the unhealthy specimens due to the higher stiffness of the healthy specimen. In cases of fractured or cracked specimens, as a comparably lower stiffness is observed, the magnitudes of vibration response tend to be higher. The magnitudes of vibration responses tend to be higher in the following order: fracture, crack and no fracture. Due to the damping effect which is similarly expected in patient, the resonances are not clear but it is analyzed that the modes appear near 50 Hz in these plastic pipe cases.

Then the SAE-based diagnosis procedure is applied to the experimental data. To achieve this, Fig. 6 presents the virtual spectrograms that are the results from the STFT processed with the difference among the FRFs. The average data of the FRFs without fracture or crack is used as a reference signal. In other words, the virtual spectrogram is generated with the difference between the average signal of the FRFs of no fracture and the one FRF signal of fracture or crack. In Fig. 6(a), the figure on the left is generated with the reference healthy signal (average healthy signal) and the healthy signal. The center figure is generated with the reference healthy signal and the crack signal, while the figure on the right is generated with the reference healthy signal and the fracture signal. In Fig. 6(b), these virtual spectrogram images show some of the data utilized by the diagnosis system. In the training process, the SAE-based diagnosis system adopts the mean square error (MSE) loss function. The left figure of Fig. 7(a) shows the convergence of the MSE of 0.056 in the autoencoder 1 and the right figure shows the approaching of the MSE of 0.022 in the autoencoder 2. It is a commonly adopted or observed fact that the increase of the number of stacks can improve the accuracy of a stacked autoencoder. In the

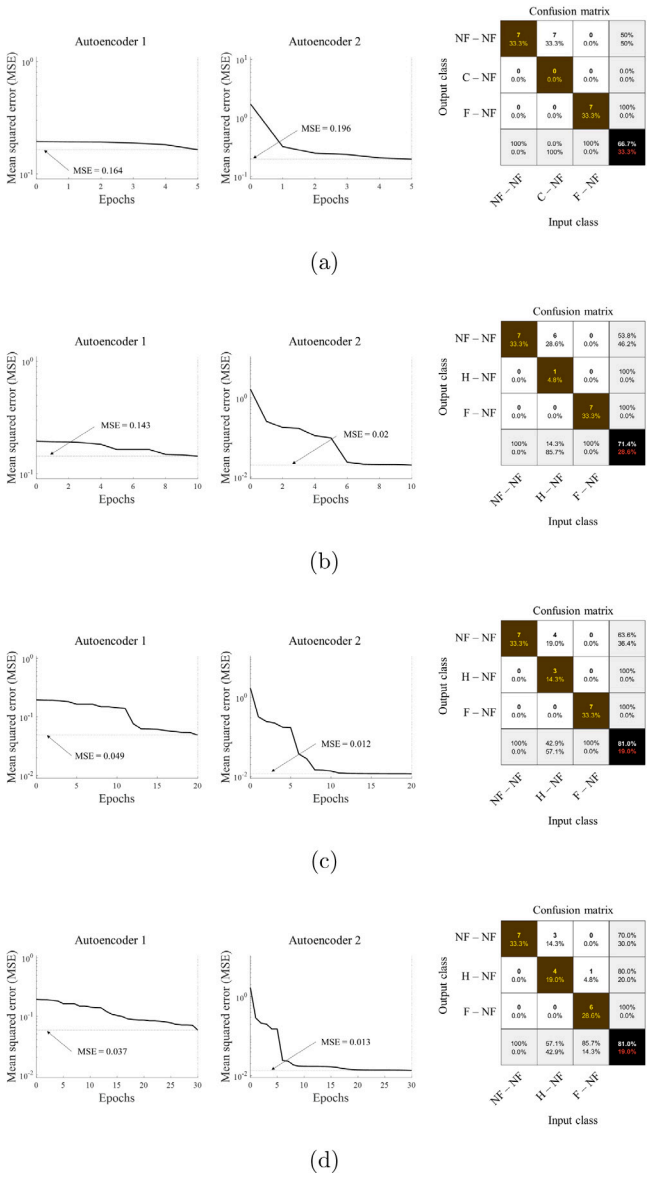


**Fig. 8.** Results of SAE with several epochs. (a-d) The results of SAE with the different epochs (a: 5 epochs, b: 10 epochs, c: 20 epochs and d: 30 epochs).

present study, we conclude that the two layers are enough for this kind of problem. Although the MSE can be lowed with more epochs, but in our experiments, we observe that the 40 epochs for training are enough to classify the data in the present study. Fig. 7(b) shows the confusion matrices of the classified results with each of the 7 data of the three health conditions. In the presented confusion matrices, the virtual spectrograms generated by the differences between no fracture and no fracture signals are classified with 100 percent accuracy and the virtual spectrograms of differences between the fracture and no fracture signals are also classified with 100 percent accuracy. However, the crack cases are classified with 71.4 percent accuracy and the total accuracy is 90.5 percent. One of the reasons may be that the crack cases are confused with the healthy cases. The virtual spectrograms of the crack cases also look like intermediate image data between the fracture and no fracture cases. To improve the accuracy of the system, the backpropagation scheme is carried out for the fine-tuning; the fine-tuning is conducted by re-training the neural network with the training data. As a result, it is possible to improve the prediction accuracy and Fig. 7(c) shows the confusion matrices with 100 percent accuracy about the three conditions.

Moreover, Fig. 8 shows the trained results of the SAE with 5, 10, 20 and 30 epochs, respectively. It turns out that the number of epochs influences the accuracy of the autoencoder. For example, with 5 epochs, the prediction accuracy is about 66.7 percent with 0.164 for the MSE of autoencoder 1 and 0.196 for the MSE of autoencoder 2. With 5 epochs, the MSE value of the autoencoder 2 is higher than that of the autoencoder 1 and the training is not properly carried out for the improved accuracy. Therefore, 40 epochs are adopted for proper training in consistency with other examples in this study. For the validation of the present approach, the additional data of plastic pipe are classified with the trained model in Fig. 9. The averaged FRF of the new 15 FRFs with no fracture, fracture and crack cases and the 15 virtual spectrograms are presented in Fig. 9(a) and (b), respectively. With the direct utilization of the trained Stacked Autoencoder (SAE), we achieve classifications with 80 percent accuracy. Upon conducting fine-tuning, which involves retraining the pre-existing SAE network using 15 new virtual spectrograms, we achieve significantly improved classifications with an accuracy of 93.3 percent, as demonstrated in Fig. 9(c). This study presents the accurate diagnosis that can be implemented for the three conditions of plastic pipe specimens using the SAE-based diagnosis system.

### 3.2. Example 2: Cadaver legs

For the next example, a cadaver (male, 84 years old, 168 cm tall) is prepared in an anatomy laboratory in Hanyang University, Seoul, Korea, on July 2020.[1] To conduct the investigation of conditions with and without fracture, a cadaver's left leg tibia is cut at the midpoint between the tibial tuberosity and the medial malleolus and the right leg is a healthy condition. Moreover, the transverse vibration experiments of cadaver specimen are carried out with the ground contact condition. It should be mentioned that unlike the tissue and muscle of a living human, some differences exist in material properties. Fig. 10(a) and (b) show a geometric configuration of cadaver legs and the frequency response functions (FRFs) at the low-frequency domain. The responses similar to the vibration response characteristics of the plastic pipe are obtained. The eigenfrequencies of the fracture case are lower than those of no fracture case in the 10–100 Hz frequency range. The comparison of the magnitudes of the responses indicates that the magnitude of the fracture case is higher than that of the healthy case as the stiffness becomes lower. Fig. 11(a) and (b) show the representative virtual spectrograms with and without fracture cases and the datasets of the virtual spectrograms employed in the SAE-based diagnosis system. In this cadaver example, the difference between fractured and unfractured virtual spectrograms is clearly distinguishable. The computed MSE values of the autoencoder 1 and the autoencoder 2 in Fig. 12(a) are 0.059 and 0.027, respectively. The employment of the two autoencoders results in noticeably faster convergence of the MSE in this diagnosis system. After confirming the convergence of the neural network, the diagnosis results are shown with the confusion matrices in Fig. 12(b) and (c).

[1] We should mention that this data was also presented in our previous contribution (Yoon et al., 2021). As the data acquisition from cadaver requires some additional administrative processes after the modification of the IRB(Institutional Review Board) rule and special permits, this data is re-utilized in the present paper to verify the concept of the SAE which is one of the unsupervised learning.

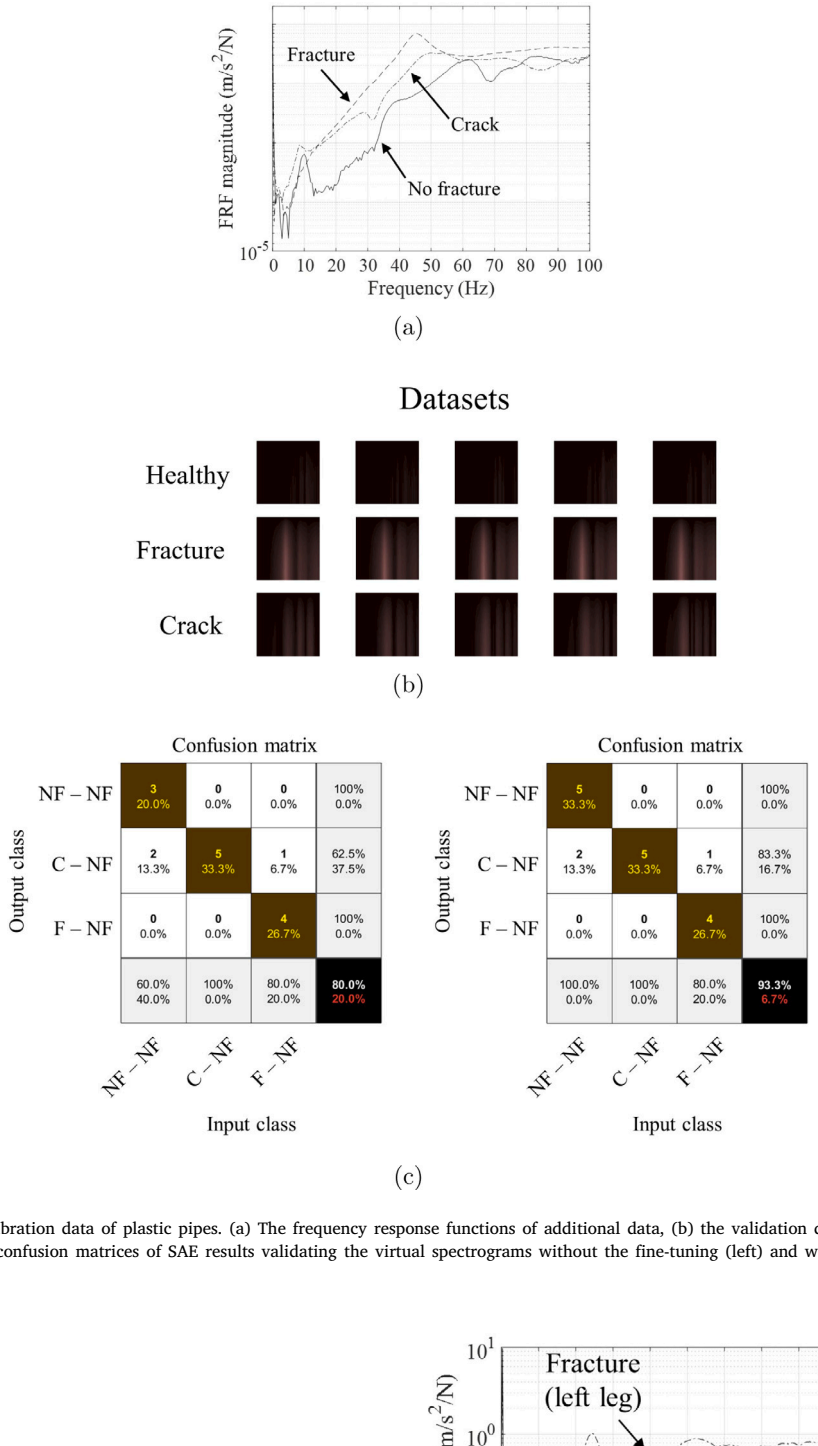


**Fig. 9.** Validation with additional vibration data of plastic pipes. (a) The frequency response functions of additional data, (b) the validation datasets of virtual spectrograms used in the diagnosis system and (c) the confusion matrices of SAE results validating the virtual spectrograms without the fine-tuning (left) and with fine-tuning (right).

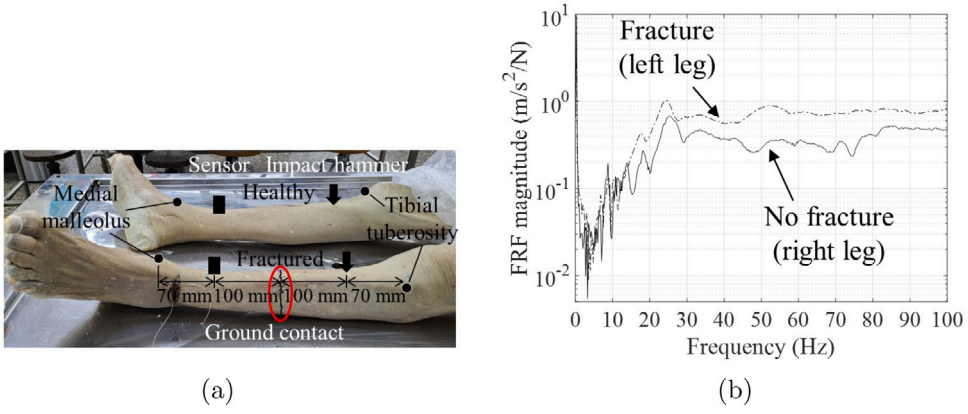


**Fig. 10.** Experiments of cadaver legs. (a) The geometric configuration of cadaver legs and (b) the FRFs without fracture and with fracture.

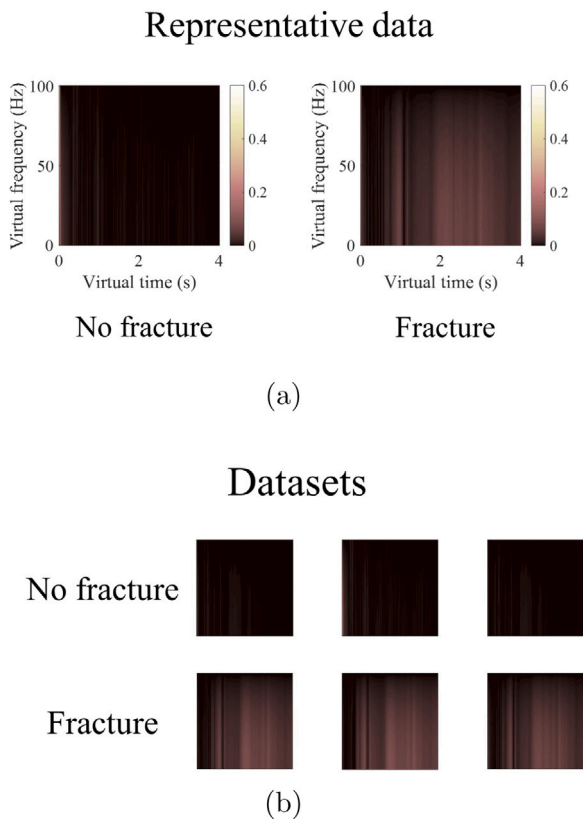


**Fig. 11.** Virtual spectrograms of the stacked autoencoder-based diagnosis system to identify the conditions of cadaver legs. (a) The representative virtual spectrograms of the two conditions without fracture and with fracture and (b) the datasets of virtual spectrogram images used in the presented diagnosis system.

### 3.3. Example 3: SAE application for patient data

To show the application of the SAE-based diagnosis system further, this section shows the measurement and analysis of a patient with a fractured bone at his right leg who has an orthopedic surgery (August 9, 2021, Hanyang University Hospital, Seoul, South Korea). The patient is a 43 years old male with 187 cm height and 100 kg weight. During the operation, an intramedullary nail made of titanium alloy is used to connect and fix his broken bones. As the patient can lie stably on a bed, the boundary condition is set to the ground contact condition. Fortunately, his left leg is intact and utilizing the bilateral symmetry, the response of his left leg is set as a reference signal in Fig. 13(a). As expected, the structural rigidity of the injured right leg has deteriorated and the response is naturally higher than that of no fracture following the law of physics, i.e., displacement responses are inversely proportional to dynamic stiffness in Fig. 13(b). The eigenfrequencies of the fracture signal are lower than those of no fracture. In short, the two curves (fracture and no fracture) show the typical characteristics of the fracture on the human leg.

The experiment after the implant operation is strictly not permitted to prevent possible infection and further injury. Therefore, after two months (2021-10-26), the experiment of the healing right leg is carried out to measure the vibration response in Fig. 13. It is interesting that the magnitudes of the response curve of the healing bone are not between those of the fractured bone and the no fracture bone in the frequency domain as shown in Fig. 13(b). The response of the healing bone with the nail is very similar to that of no fracture. From the consultant of the orthopedic doctors who are the authors of this paper, it turns out that it does not mean that two months are enough for the curing process; in hospitals in the Republic of Korea, normally it takes one year for a medical doctor to remove nail without knowing one year is sufficient and enough to heal bone and to our best knowledge, it is applied to other nations too. Rather it implies that the implanted intramedullary nail sufficiently supports the fractured leg from a structural point of view. The stiffness and strength of the implanted intramedullary nail are high enough to fix and connect the fractured bones which is the reason for the usage of the intramedullary nail from a medical and mechanical point of view. Now the SAE process can be applied to the three response curves and this also arises a new challenge to the SAE process.

The virtual spectrograms of the signals of the left leg and the right leg before and after the medical operation are shown in Fig. 14(a) and (b). To identify the three different conditions of the patient's legs, the virtual spectrograms are generated by the difference between no fracture of the left leg (2021.08.09) as the reference signal, a fracture signal of the right leg (2021.08.09) and the healing process of the right leg (2021.10.26) in Fig. 14 in order to observe the evolution of the signals as times goes by. In Fig. 14(a), it is possible to identify the healing process by comparing the virtual spectrogram of the fracture case. The SAE diagnosis system is trained and tested with these virtual spectrograms. The MSE values of autoencoder 1 and autoencoder 2 are converged to 0.053 and 0.036, respectively. The training process is carried out in each of the two autoencoders with 40 epochs and it is confirmed that the three classification cases are well diagnosed with the confusion matrices in Fig. 15(b) and (c). As shown here and discussed in the previous example, it is possible to classify the cases accurately and this proves that the SAE which is one of the unsupervised learning algorithms is effective to classify the cases.

### 3.4. Example 4: Estimation of the healing process with fractured two legs (operation only to the right leg and the natural healing process of the left leg)

As the present SAE-based diagnosis method can detect the evolution of the mechanical condition of fracture bone, it is also possible to track the healing process. After the medical operation, it is difficult to take MRI or CT regularly from a medical or economic point of view. From clinical data, it is known that it takes over one year to heal a fractured bone and it is common for orthopedic doctors to remove the implant after one year, as mentioned. As the present SAE diagnosis system is based on the simple vibration test, it turns out that it can provide some valuable clinical data to orthopedic doctors and patients. To verify this concept, another volunteer patient with the two leg fractures (55 years old, 177 cm height, 75 kg) is chosen and his data are analyzed with the SAE system; The example 3 being our first trial, it is only possible to measure the data before and after the orthopedic operation by following the relevant law and the strict IRB(Institutional Review Board) agreement. It is also an interesting case for our system as the two legs (Right leg: fracture of his right tibia and shaft fracture of right fibula, left leg: shaft fracture of the left fibula) are broken and the bilateral symmetry cannot be applied. Fig. 16(a) shows the images in case of the fracture. The medical doctor decides to implant the intramedullary nail to the right leg as the fracture of the right leg is severe and the left leg can be healed naturally. Fig. 16(b) and (c) show the responses of the right leg and the left leg. The followings are our observations.

- Firstly, the magnitudes of the fracture on the right leg are greater than those of the left leg, indicating that the damage to the right leg is more severe than that of the left leg on 2022.09.21.
- By implanting an intramedullary nail in the right leg, the stiffness of the leg can be improved. The response of the right leg on 2022.10.20 is similar to that of the patient in Example 3 after the operation.
- The curves for the healing right leg on 2022.10.20 and the healing right leg on 2023.03.23, show that the natural healing process increases the stiffness and strength of the right leg.

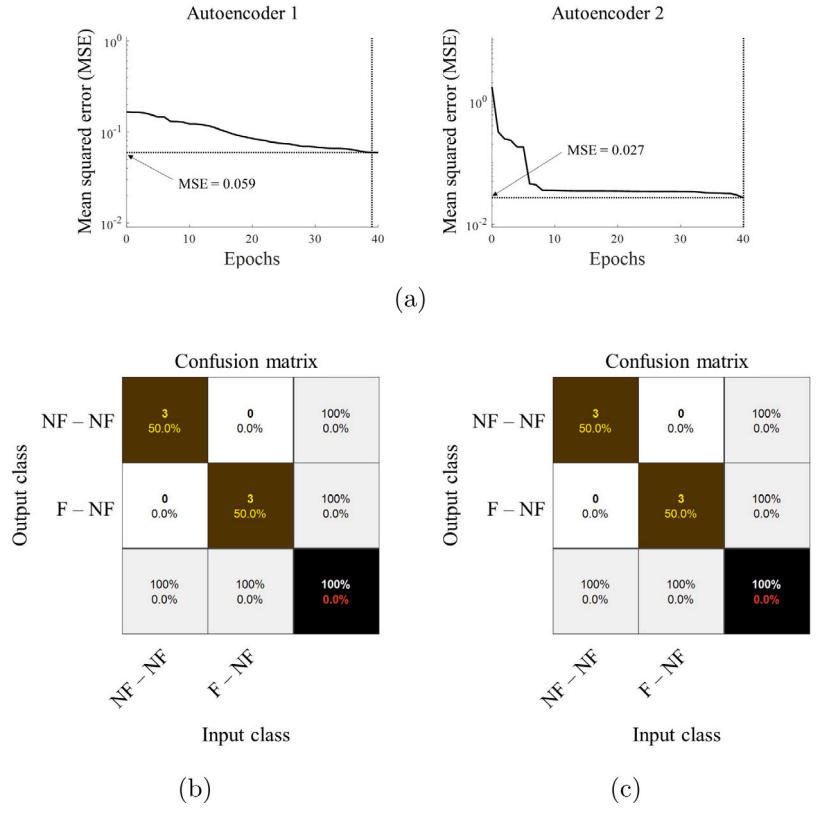


**Fig. 12.** Results of each process using the stacked autoencoder. (a) The MSEs of autoencoder 1 and autoencoder 2 with 40 epochs, (b) the confusion matrices of stacked autoencoder results testing the virtual spectrograms without the fine-tuning and (c) the confusion matrices of stacked autoencoder results testing the virtual spectrograms with the fine-tuning (NF: No fracture and F: Fracture).

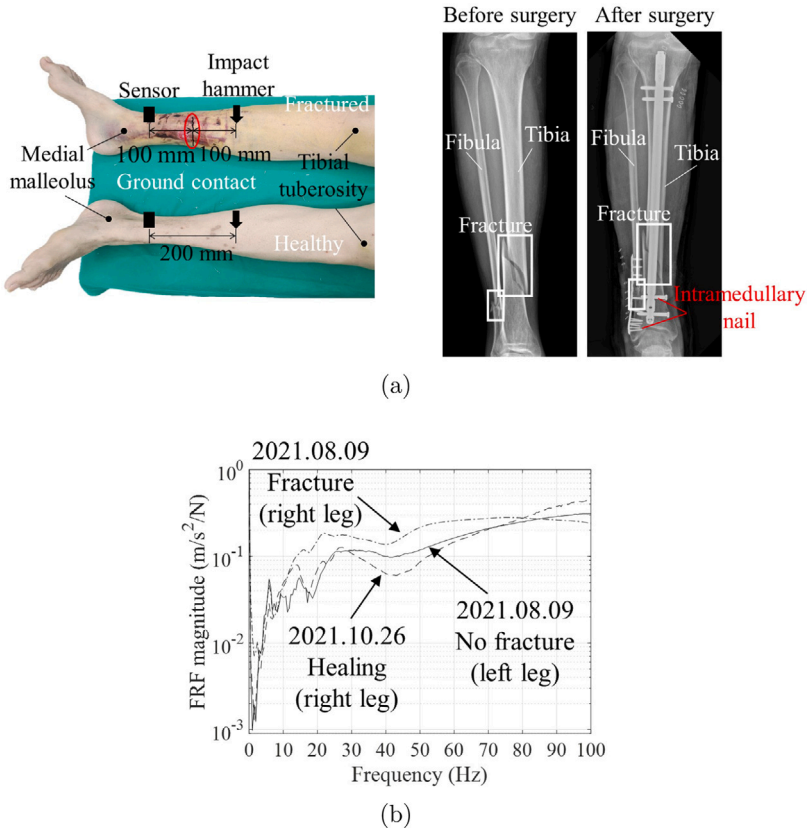


**Fig. 13.** Experiments of human legs. (a) The geometric configuration of the patient's legs (left) and the X-ray images before and after surgery of the right leg (right) and (b) the FRFs without fracture, with fracture and with the healing process.

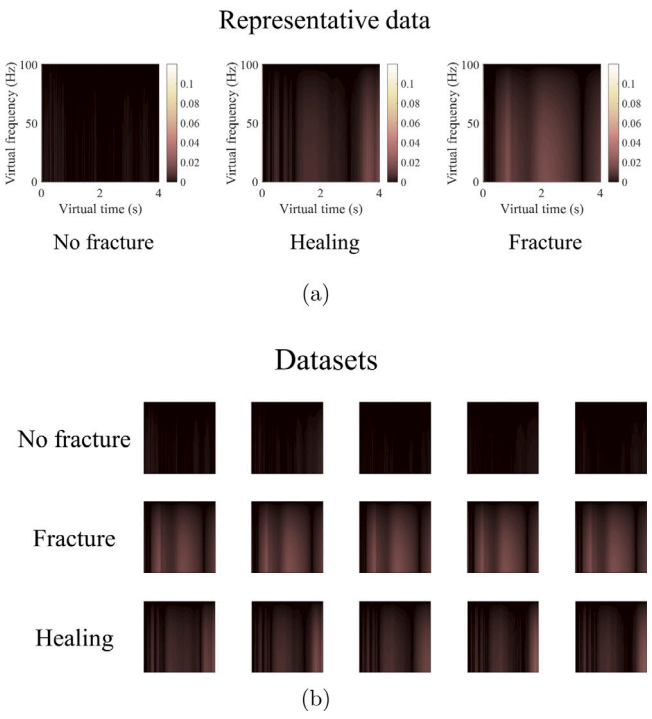


**Fig. 14.** Virtual spectrograms of the stacked autoencoder-based diagnosis system to identify the conditions of human legs. (a) The representative virtual spectrograms of the three conditions without fracture, with fracture and with the healing process and (b) the datasets of virtual spectrogram images used in the presented diagnosis system.

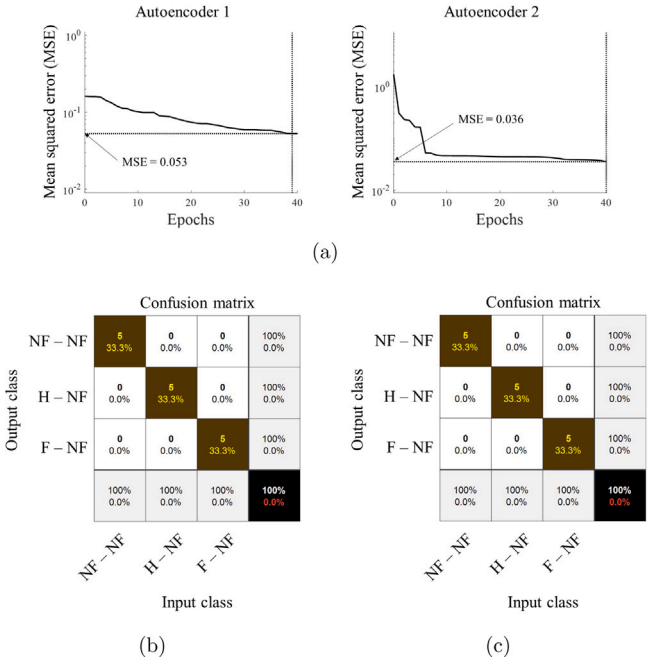


**Fig. 15.** Results of each process using the stacked autoencoder. (a) The MSEs of autoencoder 1 and autoencoder 2, (b) the confusion matrices of stacked autoencoder results testing the virtual spectrograms without the fine-tuning and (c) the confusion matrices of stacked autoencoder results testing the virtual spectrograms with the fine-tuning (NF: No fracture, F: Fracture and H: Healing).

- The curves for the fracture (left leg) on 2022.09.21 and the healing left leg on 2023.03.23, demonstrate that the left leg is fractured.
- The curves for 2022.10.20 healing (right leg), 2023.03.23 healing (right leg), 2022.10.20 healing (left leg), and 2023.03.23 healing (left leg) indicate that the curves shift towards the right side as stiffness increases over time

During the healing process, it is observed that the curve is shifted towards the right side due to the increase in stiffness over time; bone becomes stronger. However, despite the healing, the signal becomes different from the healthy signal due to the influence of the stiffness and mass of the implanted intramedullary nail. It is difficult to determine whether the leg is healed completely or not before the experiment during the removal operation of the intramedullary nail. In this diagnosis system, we need reference data such as reference no fracture in the

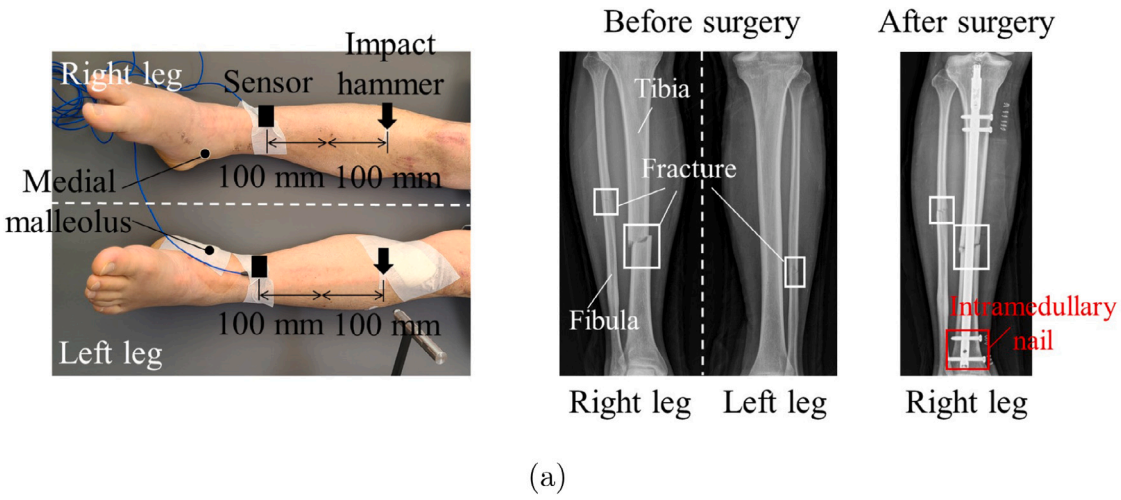


(a)

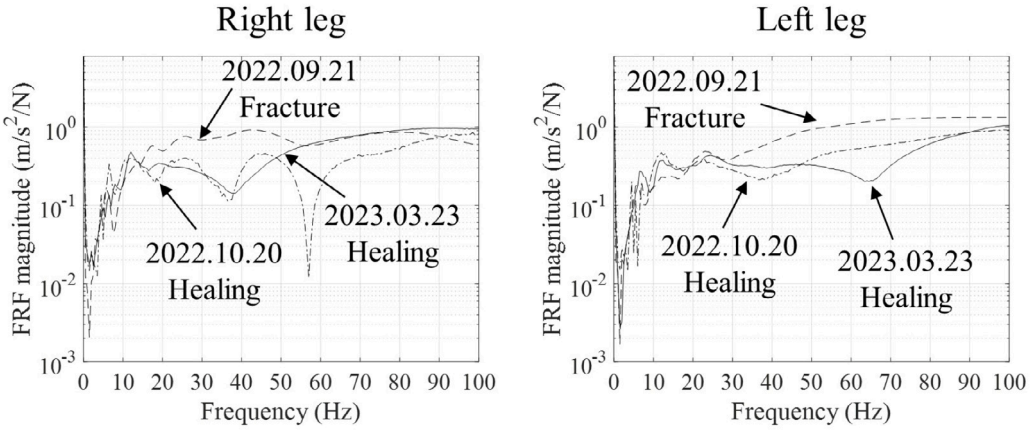


(b)

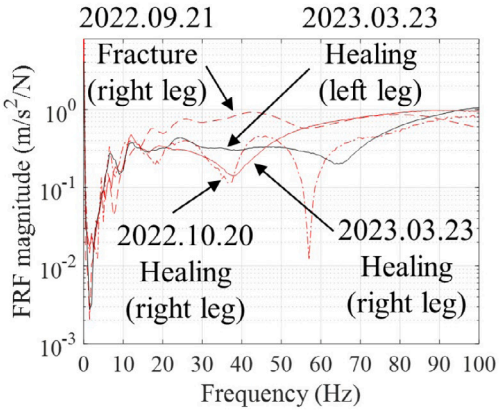


(c)

**Fig. 16.** Experiments of human with fractured two legs. (a) The geometric configuration of the patient's legs, (b) the FRFs with fracture and healing process cases of right and left legs and (c) the FRFs with fracture and healing process of the right leg including FRF of the left leg on 2023.03.23 for the concept of bilateral symmetry.

previous examples. Herein, according to the medical doctor's opinion, the patient's left leg on 2023.03.23 is almost cured, so we selected this data as a reference; After that, when the right leg is completely healed, it will be inserted for data comparison.

Fig. 17 shows virtual spectrograms of no fracture, healing after 6 months, healing after 1 month and fracture cases generated with the left leg condition on 2023.03.23 as a reference data. In Fig. 17, although virtual spectrograms of all cases are distinguishable, it is difficult to identify the healing process over time. In other words, the healing process seems to be between no fracture and fracture, but it is not easy to understand the order of fracture, healing after 1 month, healing after 6 months and no fracture. To solve this problem, the SAE-based diagnosis system can accurately classify each case. Fig. 18(a) show the MSE of 0.047 in the autoencoder 1 and of 0.039 in the autoencoder

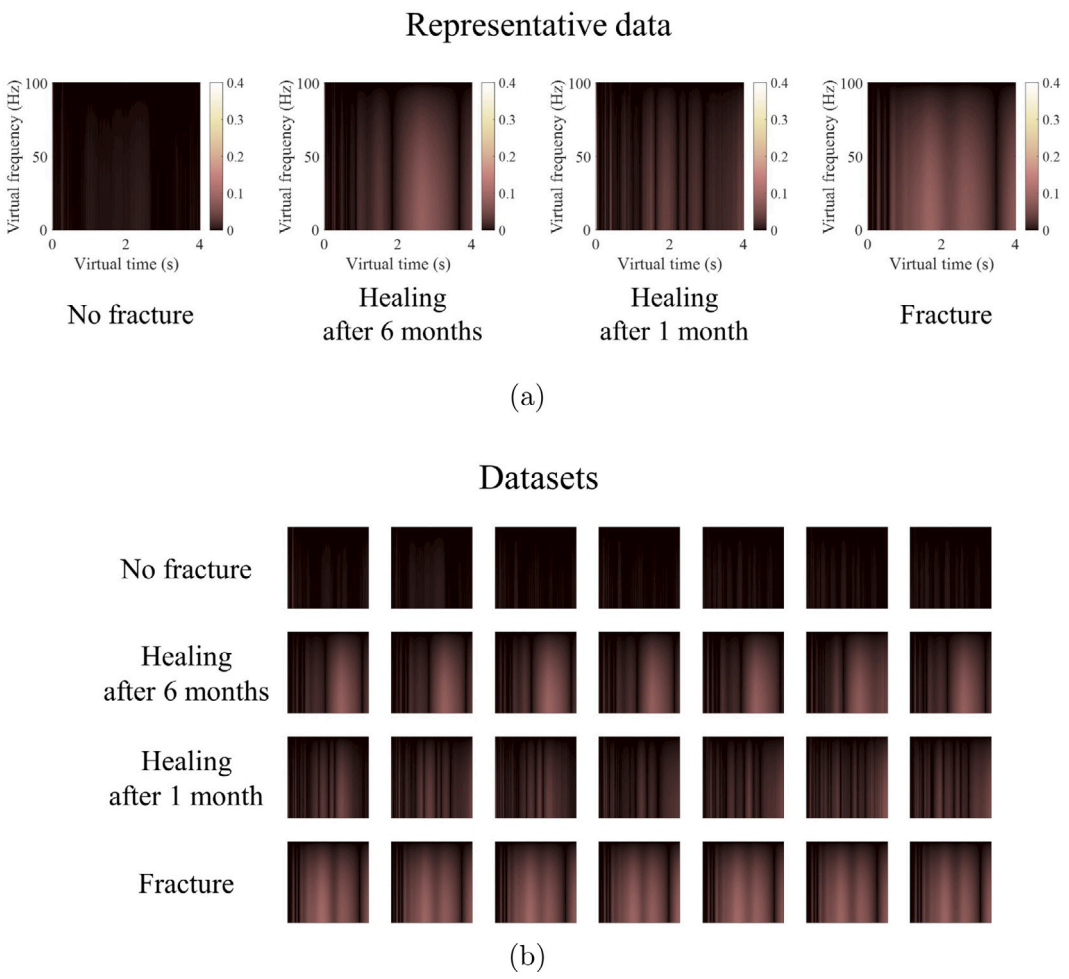


**Fig. 17.** Virtual spectrograms of the stacked autoencoder-based diagnosis system to identify the conditions of the human with fractured two legs. (a) The representative virtual spectrograms of the four conditions without fracture, with fracture and with the healing process and (b) the datasets of virtual spectrogram images used in the presented diagnosis system.

2. In Fig. 18(b) and (c), four different conditions of patient with both legs fractured are diagnosed with 100 percent accuracy. Although the present approach has the difficulty in determining the size of fracture quantitatively, it is possible to investigate the fracture by discerning the difference between the vibration-based response containing the structural stiffness degradation characteristic of the fractured leg and that of the healthy leg using the bilateral symmetry. In addition, the difference is transformed into the virtual spectrogram and can be investigated in the unsupervised learning-based stacked autoencoder. In this paper, we are able to verify the applicability of the SAE-based diagnosis method that is considered from pipes to humans using bilateral symmetry and low-frequency vibration.

## 4. Conclusions

This study has demonstrated the application of the stacked autoencoder (SAE)-based diagnosis method for the investigation of bone fracture. Achieving accurate health monitoring requires considering various physical interactions among tissue, muscle, wave propagation and boundary conditions within the human body. In addition, the absence of advanced medical devices like CT, X-ray and MRI systems poses a challenge to the investigation of fracture, crack and healing process. To address these challenges, our research proposes the SAE approach that incorporates the bilateral symmetry of human legs and leverages low-frequency transverse vibration. The utilization of virtual spectrograms, generated by differences of frequency response functions, further enhances the diagnosis capabilities of the proposed system. The presented method is validated with experiments involving the plastic bar, the cadaver and the legs of two patients. In the pipe experiments and the cadaver experiment, saws are employed to induce fractures. Consequently, an intact examination of the eye or hand can be conducted. This study focuses on the decline in stiffness, and the current method can be utilized to categorize fracture cases without the need for medical devices. The confusion matrices of diagnosis results exhibited a high accuracy for the plastic pipe, the cadaver and two humans. Fine-tuning is also applied to improve the accuracy of the above results. Finally, we achieved the accuracy of over 93.3 percent, reaffirming the potential of this SAE-based diagnosis method with respect to bilateral symmetry and low-frequency vibration responses. One of the inherent limitations of this study is that the effect of fracture or partial fracture on stiffness is not quantified and the FRF curves with and without fracture are compared and assessed relatively. This is partially inevitable by the shortage of the available data in human. With the availability of the accumulated data regarding the relationship between various sized and shaped fractures and their FRF curves, the present SAE approach can be extended to study and quantify the effect of the size or shape of the fracture. For forthcoming research, the present method can be extended to automatically perform the vibration experiment for the investigation of various fractures with the different

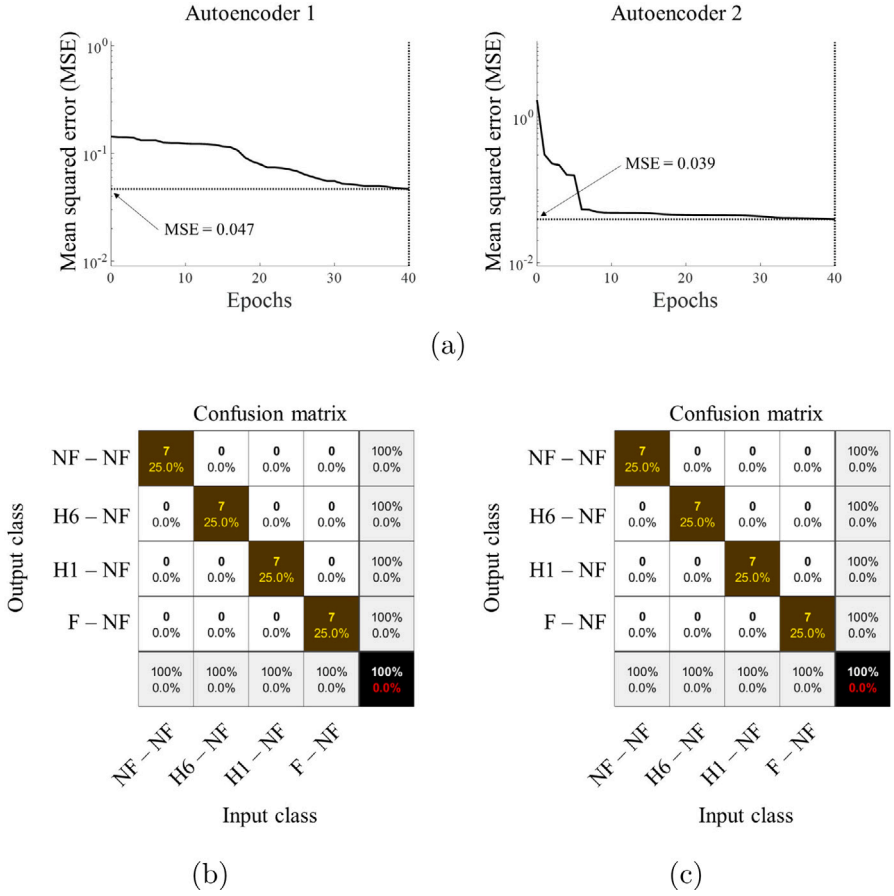


**Fig. 18.** Results of each process using the stacked autoencoder. (a) The MSEs of autoencoder 1 and autoencoder 2, (b) the confusion matrices of stacked autoencoder results testing the virtual spectrograms without the fine-tuning and (c) the confusion matrices of stacked autoencoder results testing the virtual spectrograms with the fine-tuning (NF: No fracture, F: Fracture, H1: Healing after 1 month and H6: Healing after 6 months).

boundary conditions and accurately estimate the effect of implant during the healing process.

## CRediT authorship contribution statement

**Dong-Yoon Kim:** Writing – original draft, Visualization, Validation, Methodology, Investigation, Formal analysis, Conceptualization. **Eun-Bin Park:** Visualization, Investigation, Formal analysis. **KyoBeom Ku:** Investigation, Formal analysis. **Se Jin Hwang:** Supervision, Resources. **Kyu Tae Hwang:** Supervision, Resources, Investigation. **Chang-Hun Lee:** Supervision, Resources, Funding acquisition, Formal analysis. **Gil Ho Yoon:** Writing – review & editing, Validation, Supervision, Methodology, Funding acquisition, Formal analysis, Conceptualization.

## Declaration of competing interest

The authors declare that they have no known competing financial interests or personal relationships that could have appeared to influence the work reported in this paper.

## Data availability

Data will be made available on request.

## Acknowledgments

The authors express thanks to the donor of the cadaver for the experiment and are grateful for the financial support received from the National Research Foundation (NRF) of Korea grant funded by the Korea government (MSIT) (No. 2018R1A5A7025522 and NRF-2020R1A2C2101353).

## References

Adem, K., Kiliçarslan, S., Cömert, O., 2019. Classification and diagnosis of cervical cancer with stacked autoencoder and softmax classification. Expert Syst. Appl. 115, 557–564.

Akkus, O., Korkusuz, F., Akin, S., Akkas, N., 1998. Relation between mechanical stiffness and vibration transmission of fracture callus: an experimental study on rabbit tibia. Proc. Inst. Mech. Eng. [H] 212 (5), 327–336.

Alizad, A., Walch, M., Greenleaf, J.F., Fatemi, M., 2006. Vibrational characteristics of bone fracture and fracture repair: application to excised rat femur.

Bagaria, R., Wadhwani, S., Wadhwani, A.K., 2021. Bone fractures detection using support vector machine and error backpropagation neural network. Optik 247, 168021.

Barra, V., Boire, J.Y., 2001. A general framework for the fusion of anatomical and functional medical images. NeuroImage 13 (3), 410–424.

Bediz, B., Özgüven, H.N., Korkusuz, F., 2010. Vibration measurements predict the mechanical properties of human tibia. Clin. Biomech. 25 (4), 365–371.

Bizzoca, D., Vicenti, G., Caiaffa, V., Abate, A., De Carolis, O., Carrozzo, M., Solarino, G., Moretti, B., 2020. Assessment of fracture healing in orthopaedic trauma. Injury.

Cao, G., Li, Y., Wu, S., Li, W., Long, J., Xie, Y., Xia, J., 2023. Clinical feasibility of MRI-based synthetic CT imaging in the diagnosis of lumbar disc herniation: a comparative study. Acta Radiol. 02841851231169173.

Caron, R., Londono, I., Seoud, L., Villemure, I., 2023. Segmentation of trabecular bone microdamage in Xray microCT images using a two-step deep learning method. J. Mech. Behav. Biomed. Mater. 137, 105540.

Chitkara, P., Anne, R., Lavianlivi, S., Lehto, S., Kolla, S., 2013. Imaging review of adolescent tibial tuberosity fractures. Open J. Med. Imag. 2013.

Chiu, W., Ong, W., Russ, M., Fitzgerald, M., 2017. Simulated vibrational analysis of internally fixated femur to monitor healing at various fracture angles. Procedia Eng. 188, 408–414.

Conceição, C., Completo, A., dos Santos, M.P.S., 2022. Altering the course of fracture healing monitoring. Biomed. Eng. Adv. 100068.

Dos Santos, I.M.G., Herrero, C.F.P.d.S., Pratali, R.d.R., Agnollitto, P.M., Waib, F.F., Nogueira-Barbosa, M.H., 2023. Agreement on mri diagnosis in compressive malignant vertebral fractures. Acta Ortopédica Brasileira 31, e258926.

He, S., Zhao, W., Zhang, L., Mi, L., Du, G., Sun, C., Sun, X., 2017. Low-frequency vibration treatment of bone marrow stromal cells induces bone repair in vivo. Iran. J. Basic Med. Sci. 20 (1), 23.

Hinton, G.E., Salakhutdinov, R.R., 2006. Reducing the dimensionality of data with neural networks. Science 313 (5786), 504–507.

Hosseinpour-Zarnaq, M., Omid, M., Biabani-Aghdam, E., 2022. Fault diagnosis of tractor auxiliary gearbox using vibration analysis and random forest classifier. Inf. Process. Agric. 9 (1), 60–67.

Iyer, S., Blair, A., White, C., Dawes, L., Moses, D., Sowmya, A., 2023. Vertebral compression fracture detection using imitation learning, patch based convolutional neural networks and majority voting. Inf. Med. Unlocked 38, 101238.

Jacob, N.E., Wyawahare, M., 2013. Survey of bone fracture detection techniques. Int. J. Comput. Appl. 71 (17).

Khamparia, A., Saini, G., Pandey, B., Tiwari, S., Gupta, D., Khanna, A., 2020. KDSAE: Chronic kidney disease classification with multimedia data learning using deep stacked autoencoder network. Multimedia Tools Appl. 79, 35425–35440.

Kim, D.Y., Woo, Y.J., Kang, K., Yoon, G.H., 2022. Failure diagnosis system using a new nonlinear mapping augmentation approach for deep learning algorithm. Mech. Syst. Signal Process. 172, 108914.

Kramer, M.A., 1991. Nonlinear principal component analysis using autoassociative neural networks. AIChE J. 37 (2), 233–243.

Kramer, M.A., 1992. Autoassociative neural networks. Comput. Chem. Eng. 16 (4), 313–328.

Lu, C., Wang, Z.Y., Qin, W.L., Ma, J., 2017. Fault diagnosis of rotary machinery components using a stacked denoising autoencoder-based health state identification. Signal Process. 130, 377–388.

Mahesh, M., 2001. Fluoroscopy: patient radiation exposure issues. Radiographics 21 (4), 1033–1045.

MATLAB, 2021. Deep Learning Toolbox Version 14.2 (R2021a). The MathWorks Inc., Natick, Massachusetts.

Mattei, L., Di Fonzo, M., Marchetti, S., Di Puccio, F., 2021. A quantitative and non-invasive vibrational method to assess bone fracture healing: A clinical case study. Int. Biomech. 8 (1), 1–11.

Møller, M.F., 1993. A scaled conjugate gradient algorithm for fast supervised learning. Neural Netw. 6 (4), 525–533.

Nicholson, J., Yapp, L., Keating, J., Simpson, A., 2021. Monitoring of fracture healing. Update on current and future imaging modalities to predict union. Injury 52, S29–S34.

Noshad, Z., Javaid, N., Saba, T., Wadud, Z., Saleem, M.Q., Alzahrani, M.E., Sheta, O.E., 2019. Fault detection in wireless sensor networks through the random forest classifier. Sensors 19 (7), 1568.

Olshausen, B.A., Field, D.J., 1997. Sparse coding with an overcomplete basis set: A strategy employed by V1? Vis. Res. 37 (23), 3311–3325.

Pan, X., Yang, T., Xiao, Y., Yao, H., Adeli, H., 2023. Vision-based real-time structural vibration measurement through deep-learning-based detection and tracking methods. Eng. Struct. 281, 115676.

Ribeiro, A., Husson, O., Drey, N., Murray, I., May, K., Thurston, J., Oyen, W., 2020. Ionising radiation exposure from medical imaging–A review of Patient's (un) awareness. Radiography 26 (2), e25–e30.

Shen, S.C.y., Fernández, M.P., Tozzi, G., Buehler, M.J., 2021. Deep learning approach to assess damage mechanics of bone tissue. J. Mech. Behav. Biomed. Mater. 123, 104761.

Sim, S.G., Woo, Y.J., Kim, D.Y., Hwang, S.J., Hwang, K.T., Lee, C.H., Yoon, G.H., 2021. Experimental study of the effect of the boundary conditions of fractured bone. J. Mech. Behav. Biomed. Mater. 124, 104801.

Sorriento, A., Chiurazzi, M., Fabbri, L., Scaglione, M., Dario, P., Ciuti, G., 2021. A novel capacitive measurement device for longitudinal monitoring of bone fracture healing. Sensors 21 (19), 6694.

Tao, S., Zhang, T., Yang, J., Wang, X., Lu, W., 2015. Bearing fault diagnosis method based on stacked autoencoder and softmax regression. In: 2015 34th Chinese Control Conference. CCC, IEEE, pp. 6331–6335.

Thürig, G., Korthaus, A., Frosch, K.H., Krause, M., 2022. The value of magnetic resonance imaging in the preoperative diagnosis of tibial plateau fractures: a systematic literature review. Eur. J. Trauma Emerg. Surg. 1–19.

Umans, H., Kaye, J.J., 1996. Longitudinal stress fractures of the tibia: diagnosis by magnetic resonance imaging. Skeletal Radiol. 25 (4), 319–324.

Vařeka, L., Mautner, P., 2017. Stacked autoencoders for the P300 component detection. Front. Neurosci. 11, 302.

Yang, A.Y., Cheng, L., Shimaponda-Nawa, M., Zhu, H.Y., 2019. Long-bone fracture detection using artificial neural networks based on line features of X-ray images. In: 2019 IEEE Symposium Series on Computational Intelligence. SSCI, IEEE, pp. 2595–2602.

Yang, Z., Xu, B., Luo, W., Chen, F., 2022. Autoencoder-based representation learning and its application in intelligent fault diagnosis: A review. Measurement 189, 110460.

Yoon, G.H., Woo, Y.J., Sim, S.G., Kim, D.Y., Hwang, S.J., 2021. Investigation of bone fracture diagnosis system using transverse vibration response. Proc. Inst. Mech. Eng. [H] 235 (5), 597–611.

Yoshida, T., Kim, W.C., Kawamoto, K., Hirashima, T., Oka, Y., Kubo, T., 2009. Measurement of bone electrical impedance in fracture healing. J. Orthop. Sci. 14, 320–329.

Zabalza, J., Ren, J., Zheng, J., Zhao, H., Qing, C., Yang, Z., Du, P., Marshall, S., 2016. Novel segmented stacked autoencoder for effective dimensionality reduction and feature extraction in hyperspectral imaging. Neurocomputing 185, 1–10.

Zhang, X., Vandamme, K., Torcasio, A., Ogawa, T., Van Lenthe, G.H., Naert, I., Duyck, J., 2012. In vivo assessment of the effect of controlled high-and low-frequency mechanical loading on peri-implant bone healing. J. R. Soc. Interface 9 (72), 1697–1704.